NASA TECHNICAL MEMORANDUM

NASA TM X-52194

NASA TM X-52194

NASA Offices and Research Centers Only

EXPERIMENTAL PERFORMANCE OF A LOW-THRUST, DIVERGENT-FLOW, CONTACT-IONIZATION ELECTROSTATIC THRUSTOR

by John F. Staggs and Walter C. Lathem
Lewis Research Center
Cleveland, Ohio

TECHNICAL PAPER proposed for presentation at Second Propulsion Joint Specialist Conference sponsored by the American Institute of Aeronautics and Astronautics
Colorado Springs, Colorado, June 13-17, 1966

NATIONAL AERONAUTICS AND SPACE ADMINISTRATION · WASHINGTON, D.C. · 1966

EXPERIMENTAL PERFORMANCE OF A LOW-THRUST, DIVERGENT-FLOW, CONTACT-IONIZATION ELECTROSTATIC THRUSTOR

by John F. Staggs and Walter C. Lathem

Lewis Research Center
Cleveland, Ohio

TECHNICAL PAPER proposed for presentation at

Second Propulsion Joint Specialist Conference
sponsored by the American Institute of Aeronautics and Astronautics
Colorado Springs, Colorado, June 13-17, 1966

NATIONAL AERONAUTICS AND SPACE ADMINISTRATION

EXPERIMENTAL PERFORMANCE OF A LOW-THRUST, DIVERGENT-FLOW, CONTACT-IONIZATION ELECTROSTATIC THRUSTOR

by John F. Staggs and Walter C. Lathem

Lewis Research Center
National Aeronautics and Space Administration
Cleveland, Ohio

ABSTRACT

An experimental electrostatic ion thrustor employing cesium on tungsten contact-ionization is described that has promise of meeting the approximate requirements for certain satellite attitude control and station keeping missions. The basic configuration presented is derived from the concept of divergent flow between coaxial cylinders. The ionizer emitting area is 1.0 cm^2 (1.52 mm chord length by 6.35 cm long). The radius of the convex emitting surface is 3.0 mm. Power efficiencies of 45% (excluding vaporizer and neutralizer powers) have been achieved at thrust levels of approximately 1.56 mN (0.35 mlb) and specific impulses near 7000 s. Typical accelerator drain currents are on the order of 2% of the beam current or less. Numerical analysis of possible electrode erosion due to charge exchange indicates that an electrode lifetime in excess of 20 000 hrs should be obtainable.

INTRODUCTION

Several contact-ionization thrustor geometries have been evaluated analytically.[1] Reported experimental evaluation to date has been limited primarily to convergent flow and plane-parallel flow geometries. This paper presents and discusses experimental performance of a thrustor based on divergent flow between coaxial cylinders.[1,2] Primary theoretical advantages of this thrustor concept are (1) increased current density at the emitter compared with other geometries so that the required emitter size and radiation power losses for a given thrust are reduced, (2) reduced ion and neutral density in the accelerator aperture where detrimental

charge exchange can occur.

The thrustor investigated has a thrust within a range that is required for attitude control and station keeping missions of satellites in the 200 to 700 kg mass range.[3]

THEORETICAL PERFORMANCE

Space-charge limited current flow between coaxial cylinders[1] can be written as

$$j_e = 4/9\epsilon_o(2q/m)^{1/2}\Phi^{3/2}(r^2\beta^2)^{-1} \qquad (1)$$

where ϵ_o is the permittivity of free space, q/m is the charge-to-mass ratio of the particle, r is the radius, Φ is the potential at radius r, and β is a nondimensional function of r/r_o where r_o is the radius of the emitter. If cesium is considered, equation (1) becomes (in SI units)

$$j_e = 4.74\times10^{-9}\Phi^{3/2}(r^2\beta^2)^{-1} \qquad (2)$$

For the ideal model, $r_o = 3.0$ mm, $r/r_o = 2$, and $\beta^2 = 0.279$. In the actual thrustor only a 30^o segment of the cylinders was used and an aperture was made in the anode cylinder. To investigate the effects of these modifications and design a suitable electrode system, an electrolytic tank analog[4] and an IBM 7094 computer program[5] were utilized. A cross-sectional sketch of the electrode shapes arrived at by these techniques is shown in Fig. 1. Also shown in Fig. 1 are typical trajectories and equipotential lines for the converged Poisson solution as obtained by the computer program. The figure shows that the ion beam occupies less than 60% of the accelerator aperture. The ion currents predicted by the numerical solution are compared with the ideal theoretical predictions of Eq. (2) in Fig. 2. The lower ion current from the computer program is due largely to the aperture effect (the bulging equipotential lines reduce the electric field strength).

As stated earlier, one of the theoretical advantages of the divergent flow concept is the reduced ion and neutral density in the aperture area. This should be reflected in a reduction in the amount of charge-exchange erosion that occurs and consequently in an extension of thrustor lifetime. In order to predict the accelerator charge-exchange erosion and thrustor lifetime, an analysis was made by utilizing both the electrolytic tank analog and the computer program. The space-charge-limited solution from the digital computer was preset on the electrolytic tank analog. The beam region was then divided into small areas and charge-exchange ion trajectories were determined from each of these areas. With the use of charge-exchange cross section data[6] and sputtering yields against incident angle and energy data,[7] the amount of electrode erosion was calculated. This analysis yielded the theoretical charge-exchange erosion patterns on the accelerator electrode shown in Fig. 3. The parameters used for the study were: beam current, 16.3 mA; neutral atom loss, 1.0%; electric field strength, 3.0×10^6 V/m; specific impulse, 8000 s; accelerator-to-focuser spacing (see Fig. 1), 2.14 mm. The figure is drawn for 20 000 hours of operation at the above conditions. Further discussion of the technique used in this study may be found in references 4, 8, and 9.

EXPERIMENTAL APPARATUS

Thrustor Design

A cross-sectional sketch of the thrustor is shown in Fig. 4 and photographs are shown in Figs. 5 and 6. The overall size of the thrustor (including a grounded shielding screen not shown in the photographs) is 2.5 by 7.5 by 14.0 cm. The total weight of the thrustor, excluding the vaporizer, is approximately 0.15 kg.

The accelerator electrode is made of copper and the focuser electrode material is molybdenum. Copper was chosen for the accelerator so that

back-sputtered material would not clog the porous ionizer. The ionizer, electrodes, and heater lead-in rods are all mounted from the stainless-steel support plate (Fig. 6), which is maintained at ionizer and focuser electrode potential. Boron nitride side plates confine the fibrous thermal insulation material. In operation, a stainless-steel grounded screen surrounded the thrustor to prevent stray electrons from reaching the thrustor.

The ionizer assembly is shown in Fig. 7. The ionizer manifold consists of a U-shaped channel of 0.127-mm-thick tungsten sheet electron-beam welded to the porous emitter. End plates, feed tube, and support tabs are of tantalum. Another U-shaped channel of tungsten is welded to the back of the manifold to form an enclosure for the heater strip (see Fig. 4). Heating the ionizer is accomplished by radiation from the strip. The ionizer assembly, which is approximately square in cross section (each side is 2.2 mm long), has an emitting surface area of 1.0 cm^2. This convex emitting surface has a radius of 3.0 mm, a chord length of 1.52 mm, and an overall length of 6.35 cm.

Test Facility

A schematic drawing of the test setup is shown in Fig. 8. Included is a wiring diagram for equipment used to operate the thrustor. The main chamber of the vacuum facility is 2.14 m long, has a 1.07 m diameter, and contains a liquid-nitrogen-cooled condenser. The facility was typically pumped to a pressure of from 5.0×10^{-7} to 3.0×10^{-6} torr during tests by a single 32-in. oil diffusion pump. Actual pressure depended on operating conditions. A 12-in.-diameter gate valve separated the main chamber from the thrustor chamber. A liquid-nitrogen-cooled condenser was also used in the thrustor chamber during tests. A more detailed description of the vacuum facility is given in Ref. 10. All thrustor electrical connections

were made through ceramic insulators at the rear of the thrustor chamber.

An isolation screen downstream of the thrustor was maintained at electrical ground to prevent electrons from reaching the thrustor chamber.

Instrumentation

The meters used in measuring beam currents and accelerator drain currents had an accuracy of ±1.0% of full scale. They were provided with multiple shunt circuits to allow full-scale current readings from 0.1 to 30 mA.

A molybdenum tipped probe assembly was used to investigate beam dispersion and to obtain a check of the total ion-beam current obtained from the meter readings. The assembly of seven buttons, each 6.35 mm in diameter, was located in the main chamber, approximately 0.47 m downstream from the thrustor. As the assembly traversed the ion beam, the currents produced by ions striking the probe buttons were recorded on x-y recorders. A discussion of the details of molybdenum tipped probe operation can be found in Ref. 11.

RESULTS AND DISCUSSION

Ionizer Current Density and Critical Temperature

In the analog studies of the thrustor optics, the focuser-to-ionizer spacing (dimension a, Fig. 1) was found to be a critical factor affecting current density. Fig. 9 shows the computer program current density as a function of total accelerating voltage Φ_a for various focuser-to-ionizer spacings. The focuser-to-accelerator spacing was held constant at 2.14 mm, and Φ_a/Φ_{net} was fixed at 2.0. The net accelerating potential between the emitter and ground is Φ_{net}. At a field strength of 3.0×10^6 v/m (Φ_a = 6420 V), the computer model current densities ranged from 143 to 210 A/m^2. A focuser-to-accelerator spacing of 1.52 mm was also considered. This closer accelerator spacing yielded slightly poorer optics and lower

thrust (due to a lower specific impulse) for the same Φ_a/Φ_{net} ratio and field strength. The accelerator aperture was held constant at 3.0 mm in all cases.

Figs. 10a and 10b show comparisons between the experimental current density and the digital computer predictions for the two focuser-to-accelerator spacings considered. The maximum current density obtained experimentally at a field strength of 3.0×10^6 V/m was 160 A/m^2. Varying Φ_a/Φ_{net} from 1.5 to 3.0 with a constant Φ_a did not significantly change the experimental current density. This result had been predicted by the computer program.

The porous tungsten used in all the tests was a high quality E-4 type[12] (spherical powder, 1 to 5 μ in diam., about 79% of theoretical density). In Fig. 11 critical temperature data on this material, as determined from pellet evaluations,[13] are compared both with data taken during thrustor operation and with the zero-field Taylor-Langmuir curve for solid tungsten,[14] The critical temperature data[13] are points of minimum neutral fraction (less than 1%), whereas the data reported herein are at temperatures at which the current density dropped to 95% of its maximum value. These two methods of determining critical temperature probably yield almost the same results, since during the tests, it was observed, that the minimum accelerator drain currents occured near this fraction of the total beam current. In the fabrication of the ionizer assemblies, many processes may affect the critical temperature. One factor, for example, is the technique used to trim the ends of the ionizer assemblies in which ordinary machine oil is used to cool the tungsten. This procedure could result in carbon contamination of the tungsten and raise the critical temperature,[15] which possibly accounts for part of the increase over the data from reference 13. Another possible factor in

increasing the critical temperature is surface sintering. Although the ionizers were chemically etched to prevent this phenomenon, this effect may have occured to a small degree. A third factor could be oxidation of the ionizer surface, which can result in an increase in critical temperature.[13]

Ionizer Heating

As stated earlier, the ionizer in the experimental thrustor is heated by radiation from a hot tungsten strip. The strip has a uniform width but varies in thickness along its length. The optimum configuration was determined empirically. The variation allows more power to be radiated to the ends of the ionizer, which lose heat by conduction through the feed tube and support tab (see Figs. 6 and 7). The chosen heater strip design produced uniformity in temperature to within 10° K over the entire ionizer. The strip heater used should not present any limit to the thrustor lifetime, barring material defects or mechanical misalignment. If zero ambient pressure and a strip temperature of 2200° K are assumed, a 1.0% resistance increases (due to evaporation of tungsten) should occur after 2.5×10^4 hours of operation. The total heater lifetime should be at least ten times this value.[16] The linear thermal expansion of the heater strip is approximately 0.63 mm. A small amount of tension on the strip, however, prevents buckling, and the heater support is capable of at least as much movement as the expansion of the strip. These two factors were the most critical in assembling and adjusting the heater.

Total experimental ionizer heater power as a function of ionizer temperature taken from several tests is shown in Fig. 12. A larger emitting area would result in a higher heating efficiency due to the less than linear increase in manifold size and conduction losses with emitting area.

Temperature cycling tests were made simultaneously on two heater designs of circular cross section (0.5 mm diam.). Each was suspended in the same manner as discussed previously and surrounded by a simulated ionizer. The tests were conducted in a bell jar facility, and the simulated ionizer temperatures were measured by thermocouples, and recorded on strip-chart recorders. The simulated ionizer temperatures were cycled between 800° and 1540° K. Approximately 3200 cycles were obtained with no apparent deterioration before an inadvertant pressure rise in the bell jar terminated the test.

Accelerator Drain Currents

Possible sources for accelerator drain currents include direct impingement, charge-exchange ion impingement, drain currents across cesium coated insulators, thermionic electron emission from a hot cesium coated accelerator, and secondary emission resulting from ion impingement.

The digital computer program predicted zero direct ion impingement. A total of 133 hrs of thrustor operation was accumulated with the complete absence of any observable accelerator erosion. The average beam current during this time was 5.7 mA.

Typical experimental data of the ratio of total accelerator drain current J_A to beam current J_B as a function of total accelerating voltage Φ_a are presented in Figs. 13 and 14. In Fig. 13, typical data are compared for three different flow rates. A possible explanation of the reversal of the slope of these curves with increasing voltage is field enhancement of thermionic emission from the cesium coated accelerator.[17] In Fig. 14, results obtained with a background pressure of 7.0×10^{-7} torr are compared with those obtained at the same mass flow rate but with a background pressure of 6.0×10^{-5} torr of oxygen. When oxygen is admitted to the system, it may change the thermionic emission characteristics of

the cesiated copper accelerator surface as well as have a decarburizing or oxidizing effect on the ionizer.[15] In every instance, the addition of oxygen reduced the accelerator drain currents. The exact mechanism of the change is not fully understood, but it is believed that the reduction in drain currents occurs too rapidly after the addition of oxygen (on the order of 1 min) to be caused by decarburization of the ionizer and is probably due to a combination of the other effects.

From the charge-exchange study discussed previously, the total charge-exchange impingement was calculated to be about 10^{12} ions/sec, or approximately 0.001% of a 16.0 mA ionizer current. Based on this value, nearly all the experimental drain currents may be attributed to thermionic electron emission from the accelerator. The neutral fraction for this calculation was assumed to be 1.0%. Two important factors affecting the neutral fraction besides the characteristics of the tungsten are (1) temperature uniformity over the ionizer and (2) matching the arrival rate of cesium at the emitting surface with the electric field at that surface. In the present ionizer, this second condition is achieved by contouring the back (the upstream face) of the porous tungsten. The final shape, shown in Fig. 15, was obtained by setting up an analog of the flow through the porous tungsten by using the electrolytic tank and a technique described in Ref. 18. In this figure, the dashed lines show the contour of the porous surfaces and the solid lines represent surfaces where the pores have been closed by electron beam welding.

Optical Characteristics

The optical characteristics of the thrustor as predicted by the analog and digital computer studies were verified by beam probe measurements. Fig. 16 shows a contour plot of the current-density variation through a

cross section of the beam 0.47 m downstream from the ionizer. The beam current, measured while these data were being taken, was 3.4 mA, which checks reasonably well with the 4.75-mA beam current calculated by rough integration of the contour plot. The difference in values could easily be due to secondary emission from the probes and/or inaccuracies in drawing the contour plot because of the limited number of probes used. Also, from the plot it was determined that 90% of the beam current lies within a dispersion angle of about 15°, which supports the analog and digital computer predictions of an 18° dispersion angle (see Fig. 1).

Overall Performance

The overall performance of the thrustor reported herein approximates the requirements for certain satellite attitude control and station keeping missions in which a thrust range of 0.445 to 1.78 mN (0.1 to 0.4 mlb) is needed.[3] These stationary-satellite missions require control systems that are light weight, efficient, and long-lived. In the continuous correction mode of operation, approximately 0.445 mN (0.1 mlb) of thrust is needed for every 160 kg of satellite weight.[3] Fig. 17 shows the thrust as a function of beam current for three different specific impulses (the thrust was calculated from measured beam currents and net-accelerating voltages). This variation in specific impulse was achieved by changing Φ_a/Φ_{net} while maintaining constant Φ_a. For two of the specific impulses the data are extrapolated to a 16.0-mA beam current (dashed lines).

Figs. 18a and 18b show power efficiencies as a function of specific impulse. These values do not include vaporizer or neutralizer powers. In Fig. 18a data are presented for an accelerator-to-focuser spacing of 1.52 mm and a beam current of 13.5 mA. The lower solid curve shows data taken early in the program over a broad range of specific impulse with

inefficient heating and at ionizer temperatures well above critical. The dashed curve indicates performance that may have been obtainable with the more recent heater design improvements and the critical temperature data of this report. Figure 18b shows data taken at two different beam currents obtained by using an accelerator-to-focuser spacing of 2.14 mm and improved heater designs. These data are projected for operation at critical temperature in the same manner as was done in figure 18a. The data include accelerator drain power losses. If the cirtical temperatures of Ref. 13 were used, instead of the critical temperatures of this report, the projections of data would yield power efficiencies above 60%.

Fig. 19 shows power-to-thrust ratios against specific impulse at different beam current levels. The lowest solid curve is a reference plot for a 100% efficient thrustor. The upper solid curves represent data. The dashed curves are projections of the data as in Fig. 18b.

A slightly larger thrustor[19] using converging flow optics shows projected power-to-thrust curves somewhat lower than given in Fig. 19. Since no raw data curves were given in Ref. 19, however, comparison of actual performance is not possible.

CONCLUSIONS

The experimental electrostatic ion thrustor discussed herein has promise of meeting the approximate requirements for certain satellite attitude control and station keeping missions. Thrust levels between 0.89 and 1.56 mN (0.2 and 0.35 mlb) were produced at power efficiencies to 45% (excluding vaporizer and neutralizer powers). The thrustor operates well at specific impulses ranging from 5000 to 8000 s. The optical characteristics are such that no primary ion impingement on the accelerator electrode occurs, and drain currents are about 2% or less of the beam current. Electrode lifetime as indicated by computer studies should be

in excess of 20 000 hr. While the potential advantage of this thrustor configuration appears to be its long electrode and heater lifetimes, improvements in ionizer heat shielding could increase considerably the power efficiency, which would result in a decrease in power-to-thrust ratio for a given specific impulse.

REFERENCES

1. Lockwood, D. L., Mickelsen, W. R., and Hamza, Vladimir, "Analytic space-charge flow and theoretical electrostatic rocket engine performance," ARS Preprint 2400-62 (1962).
2. Langmuir, I., and Blodgett, Katherine B., "Currents limited by space-charge between coaxial cylinders," Phys. Rev. 22, 347-356 (1923).
3. Molitor, J. H., "Ion propulsion system for stationary-satellite control," Spacecraft and Rockets J., 1 170-175 (1964).
4. Staggs, J. F., "An electrolytic tank analog for two-dimensional analysis of electrostatic-thrustor optics," NASA TN D-2803 (1965).
5. Hamza, V., and Richley, E. A., "Numerical solution of two-dimensional poisson equation: theory and application to electrostatic-ion engine analysis," NASA TN D-1323 (1962).
6. Marino, Lawrence L., Smith, A. C. H., and Caplinger, E., "Charge transfer between positive cesium ions and cesium atoms," Phys. Rev., 128 2243-2250 (1962).
7. Cheney, K. B., Rogers, E. E., and Pitkin, E. T., "Research on experimental evaluation of sputtering yield rates," Marquardt Corp. Rept. ARL 63-125 (July 1963).
8. Brewer, G. R., "On the nature of leakage currents in cesium contact ion engines," Hughes Res. Lab., Rept. No. 281, (August. 1963).
9. Staggs, John F., and Lathem, Walter C.: Proposed NASA TN.

10. Keller, Thomas A., "NASA Electric Rocket Test Facilities," Seventh National Symposium on Vacuum Tech. Trans. (Pergamon Press, New York, 1960), pp. 161-167.

11. Kerslake, W. R., "Accelerator grid tests on an electro-bombardment ion rocket," NASA TN D-1168 (1962).

12. Butler, C. K., "Fabrication and testing of five (5) porous tungsten blocks," Electro-Optical-Systems Rept. 5140, (Dec. 20, 1964).

13. Cho, A. Y., Hall, D. F., and Shelton, H., "Program of analytical and experimental study of porous metal ionizers," Physical Electronics Lab. TRW-4148-6013-SU-000 (NASA CR-54325)(July 15, 1965).

14. Reynolds, T. W., and Childs, J. Howard, "A graphical method for estimating ion-rocket performance," NASA TN D-466 (1960).

15. Turk R. R., and McKee, W. E., "Ion engine supporting research and evaluation," vol. 1, Hughes Res. Lab. (NASA CR-54411) (Nov. 1965).

16. Kohl, W. H., "Materials and Techniques for Electron Tubes" (Reinhold Publishing Corp., New York, 1960).

17. Wasserbauer, J. F., "Field-enhanced thermionic emission from electrodes of cesium ion thrustor," NASA TN D-2635 (1965).

18. Proposed NASA CR-54676, Hughes Res. Lab. (unpublished as of 3-30-66).

19. Anderson, J. Robert, and Thompson, S. A., "Development and long-life performance of ion engines for satellite control," AIAA Paper 66-234 (March 1966).

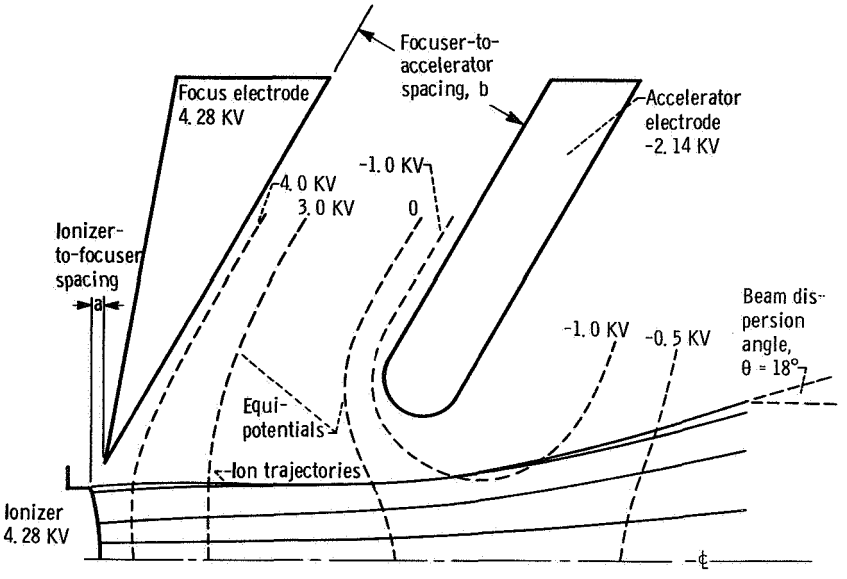

Fig. 1. - Cross section of ionizer, electrodes, and optical characteristics from digital computer program.

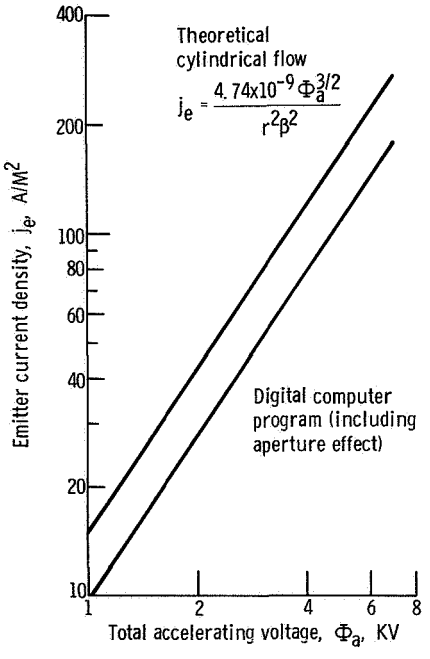

Fig. 2. - Comparison of theoretical and digital computer program current densities j_e as functions of total accelerating voltage, Φ_a.

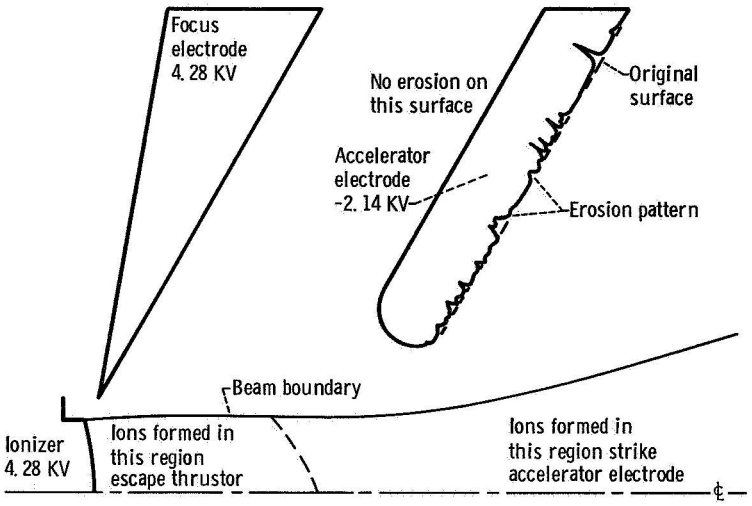

Fig. 3. - Theoretical accelerator erosion pattern due to charge exchange ion impingement after 20 000 hr at 163 A/M^2; total beam current, 16. 3 mA; neutral atom loss, 1. 0% of the total beam current.

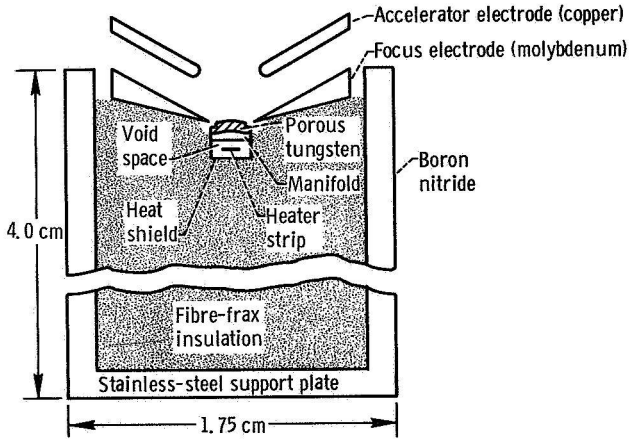

Fig. 4. - Cross section of thrustor showing overall dimensions of supporting structure and materials used.

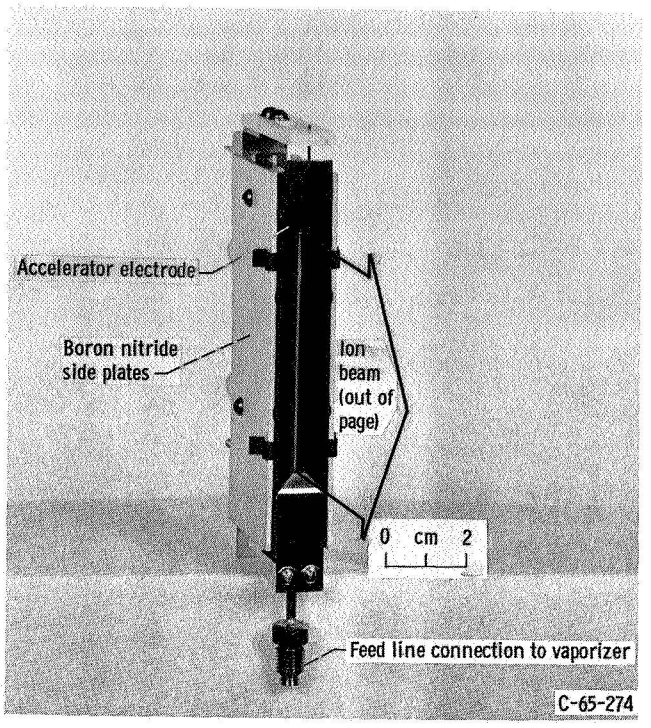

Fig. 5. - Thrustor (vaporizer not shown).

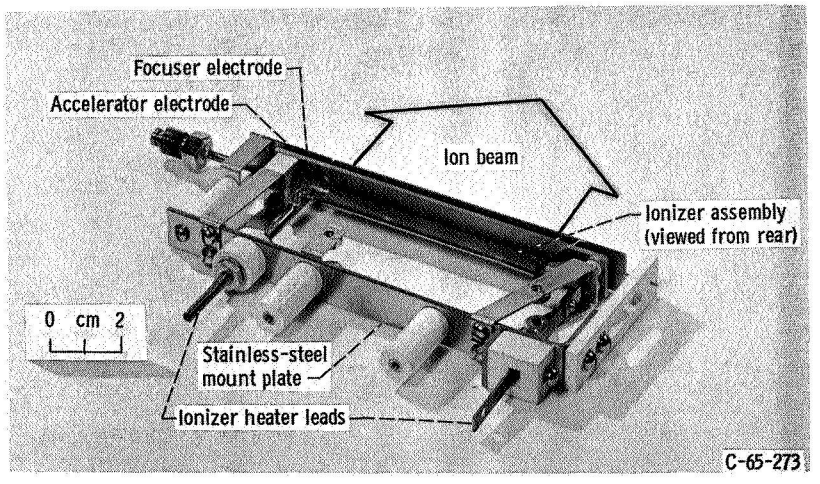

Fig. 6. - Partially disassembled thrustor.

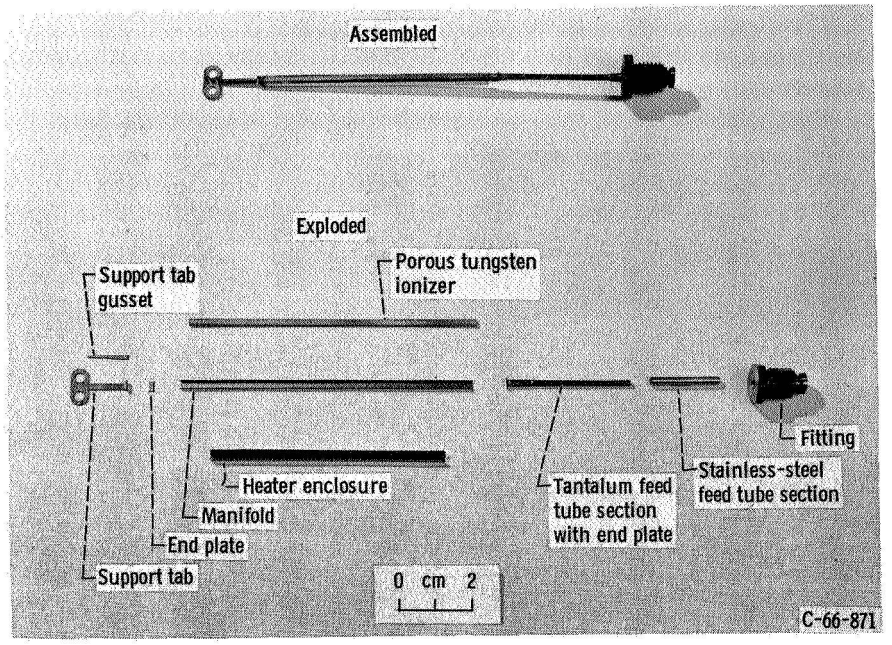

Fig. 7. - Ionizer assembly (assembled and exploded views).

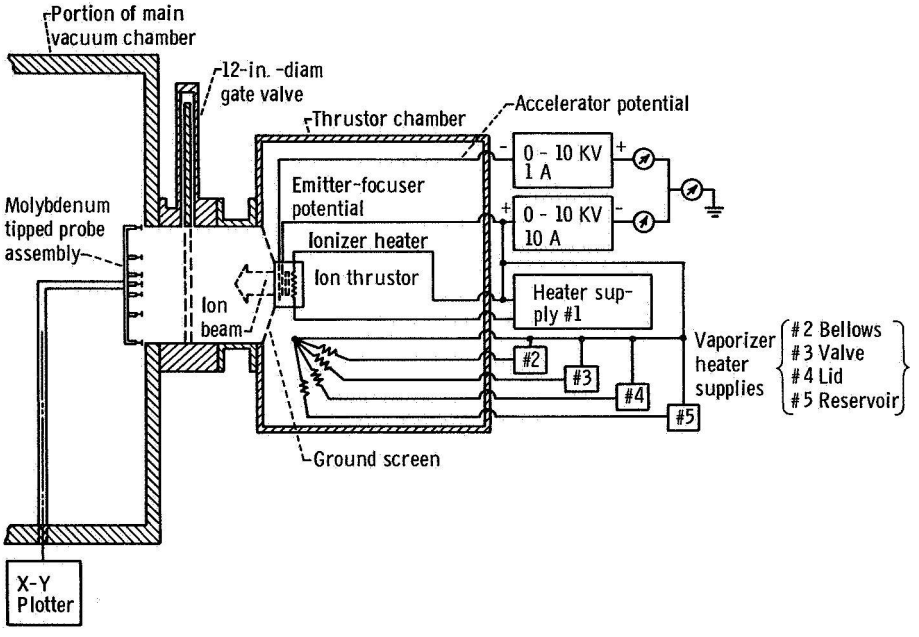

Fig. 8. - Test setup.

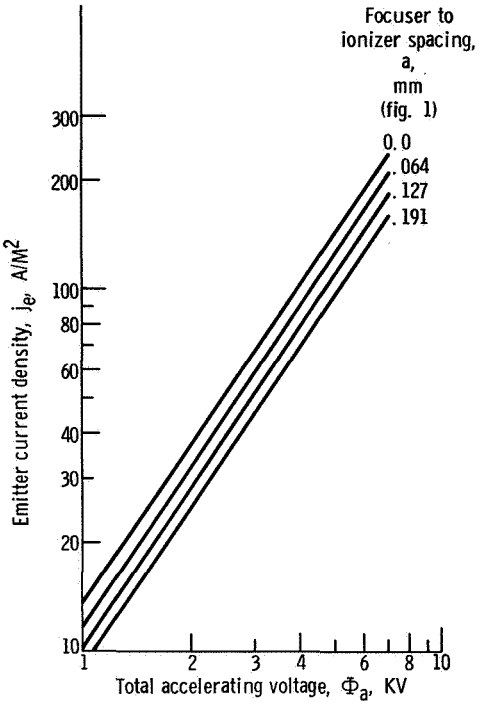

Fig. 9. - Effect of focuser-ionizer spacing, a, on emitter current density j_e from computer program. Focuser-accelerator spacing, b, 2.14 mm.

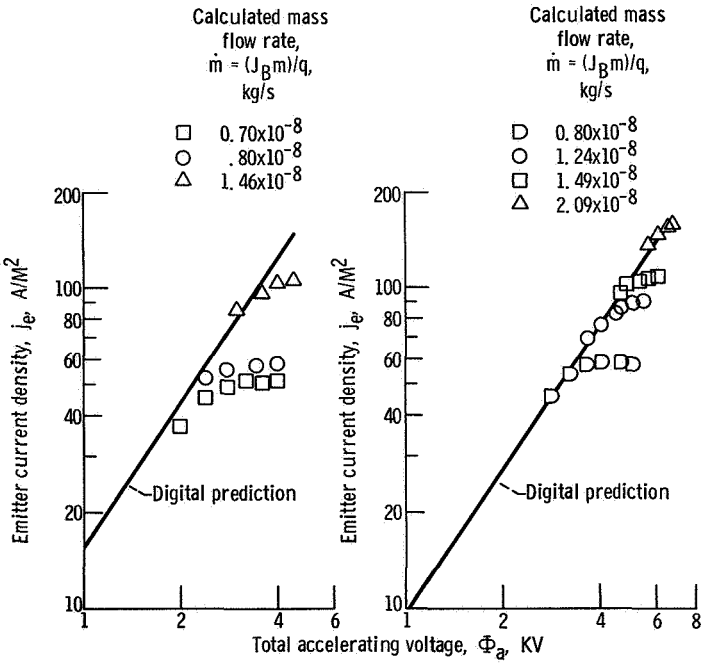

(a) Focuser-accelerator spacing, b, 1.52 mm.

(b) Focuser-accelerator spacing, b, 2.14 mm.

Fig. 10. - Comparison of experimental current densities with computer predicted values; focuser-ionizer spacing, a, 0.127 mm.

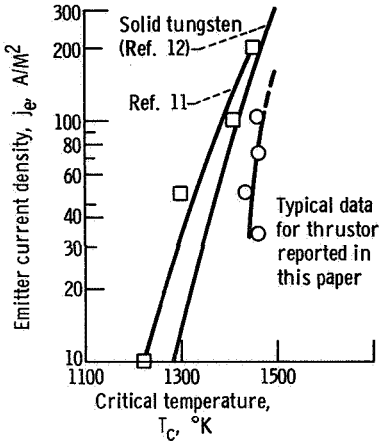

Fig. 11. - Comparison of critical temperature measurements with those of Ref. 11 and with the zero-field Taylor-Langmuir curve for solid tungsten.

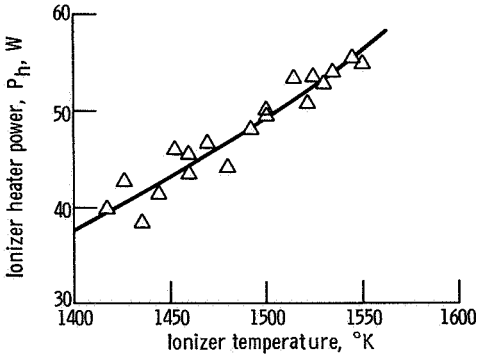

Fig. 12. - Typical experimental ionizer temperature as a function of ionizer heater power.

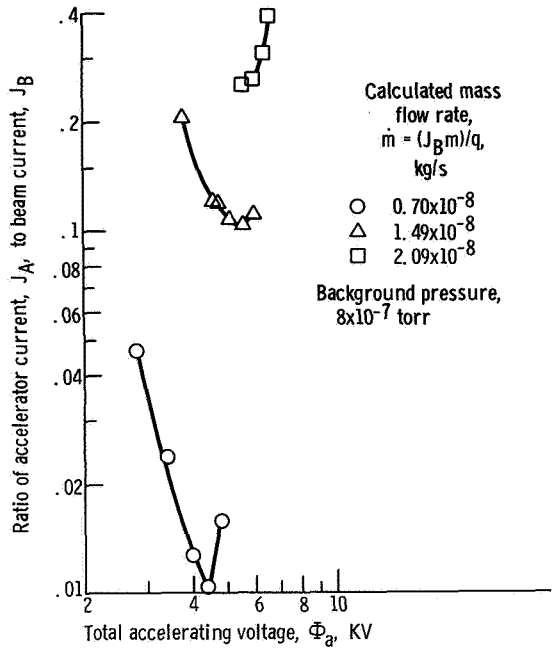

Fig. 13. - Ratio of accelerator drain current, J_A, to beam current, J_B, as a function of total accelerating voltage, Φ_a, for several mass flow rates.

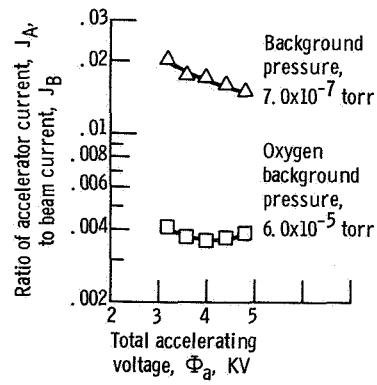

Fig. 14. - Effect of oxygen atmosphere on accelerator drain currents. Calculated mass flow rate, $\dot{m}$, 8.9×10^{-9} kg/s.

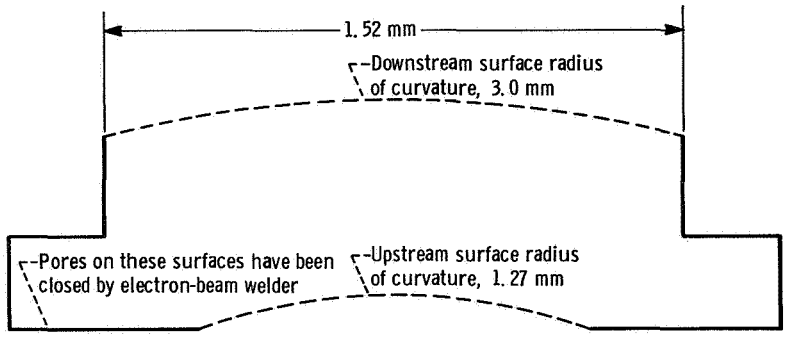

Fig. 15. - Cross section of porous tungsten ionizer showing surfaces that have been washed with an electron-beam welder.

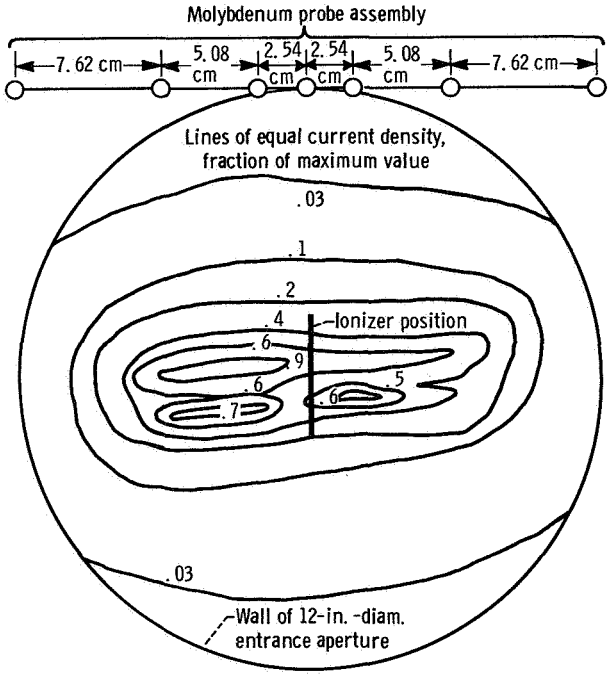

Fig. 16. - Current contour map from molybdenum button probe measurements showing lines of equal current density. Total current calculated from this figure, 4.75 mA (solid vertical bar shows projected position of ionizer).

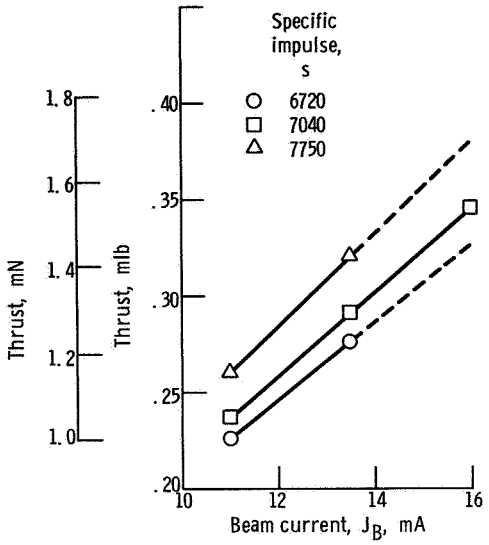

Fig. 17. - Thrust versus experimental beam current for three specific impulses.

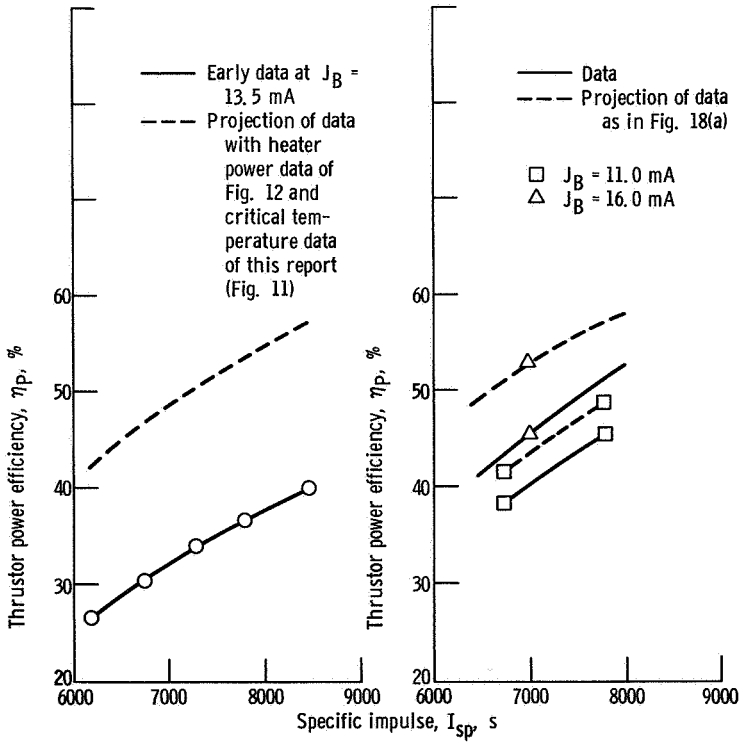

(a) Focuser-accelerator spacing, b, 1.52 mm.

(b) Focuser-accelerator spacing, b, 2.14 mm.

Fig. 18. - Thrustor power efficiency, η_P, against specific impulse, I_{sp}.

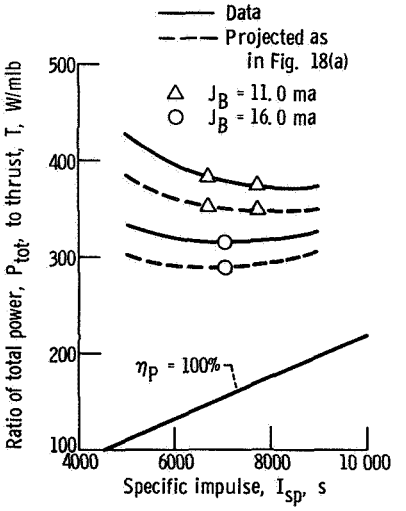

Fig. 19. - Ratio of total power expended, P_{tot}, to thrust produced, T, against specific impulse, I_{sp}.